AIAA JOURNAL
Vol. 31, No. 11, November 1993

Analysis of Instability-Related Delamination Growth Using a Crack Tip Element

Barry D. Davidson* and Todd M. Krafchak†
Syracuse University, Syracuse, New York 13244

One-dimensional delamination buckling and growth is analyzed using closed form cylindrical buckling and crack tip element analyses. A cylindrical buckling analysis is used to determine the strains, curvatures, deflections, forces, and moments in a buckled region bounded by the laminate free surface and a near-surface delamination. These results are used as input into a linear crack tip element analysis to obtain the total energy release rate and individual mode I and mode II components. Geometric nonlinearities are accounted for through the loading on the crack tip element. Total energy release rate and fracture mode ratio as found by this new technique are shown to agree with nonlinear finite element results.

Introduction

REGIONS bounded by the laminate free surface and a near-surface delamination in compression loaded composite laminates may buckle locally. This local instability, commonly referred to as delamination buckling, may create the necessary conditions for delamination growth to occur. Thus, laminate failure initiated by delamination buckling may be a critical design concern for many composite structures.

To elucidate the fundamental mechanics controlling delamination buckling and growth, a number of studies[1-7] have been conducted on laminates containing a through-width delamination. The onset of delamination buckling has been predicted by cylindrical buckling[1-4] and finite element analyses.[5-7] In the post-buckling regime, delamination growth is predicted to occur when the energy release rate G equals or exceeds its critical value G_c. For many materials, G_c is a function of fracture mode ratio.[8] Thus, prediction of the individual energy release rate components G_I and G_{II} is also important in this problem.

The value of the energy release rate in the post-buckling regime has been predicted by closed form cylindrical buckling analyses,[1-3] nonlinear finite element analyses,[5,6] and an approximate superposition analysis.[4-7] The cylindrical buckling analysis gives only the total energy release rate; fracture mode ratio cannot be obtained. The approximate superposition analysis may be used to obtain both energy release rate and mode ratio. This approach consists of a set of linear, closed form equations that use parameters, obtained by linear finite element analysis, relating the energy release rate to load and moment resultants in the post-buckled region. However, the approximate superposition analysis has been shown to underpredict the energy release rate and its individual mode I and mode II components.[6] Nevertheless, this approach has been used for qualitative investigations, because it correctly predicts "trends" in the energy release rate and mode ratio and circumvents the difficulty of obtaining nonlinear finite element results.

In this work, a recently developed technique for predicting mixed-mode energy release rates[9,10] is applied to the one-dimensional delamination buckling problem. In this technique, a crack tip element is used to obtain the energy release rate and fracture mode ratio. It is shown that a closed form, nonlinear cylindrical buckling analysis to predict local load and moment resultants, coupled with a closed form, linear analysis of the crack tip element, may be used to predict energy release rates and fracture mode ratios accurately for the one-dimensional delamination buckling problem. The accuracy of this new technique is demonstrated by comparison with nonlinear finite element results.

Cylindrical Buckling Analysis

Figure 1 illustrates the geometry that is considered. The two delaminations are assumed to exist at equal distances above and below the laminate's midplane. Referring to the figure, the term "delaminated region" is used to denote the relatively thin regions bounded by the delaminations and the laminate free surfaces, and the term "base region" is used to denote the center region bounded by the two delaminations. The term "parent laminate" is used to denote the laminate outside of the region in which the delaminations exist. It is assumed that the parent laminate possesses midplane symmetry. It is also assumed that the delaminated regions have flexural rigidities that are small compared with that of the base region, and that local buckling of the delaminated regions occurs without an associated instability in the base region.

Given the previous assumptions, the postbuckling behavior of the delaminated region may be predicted by the cylindrical buckling analysis developed by Yin.[3] It is assumed that the parent laminate is subjected to applied loads or displacements such that the midplane strains in the base region are given by

$$\epsilon_x^0 = -\epsilon_0 \qquad \epsilon_y^0 = \beta \qquad \gamma_{xy}^0 = \gamma \tag{1}$$

Considering the upper delaminated region, solutions are sought for the postbuckling deformations of the form

$$w(x) = -\frac{W}{2}(1 + \cos \lambda x) \qquad \kappa_x = -\frac{W}{2}\lambda^2 \cos \lambda x$$

$$\kappa_y = \kappa_{xy} = 0 \qquad \epsilon_x^0 = \alpha + \xi \cos \lambda x \tag{2}$$

$$\epsilon_y^0 = \beta + \zeta \cos \lambda x \qquad \gamma_{xy}^0 = \gamma + \eta \cos \lambda x$$

Received Feb. 2, 1993; revision received April 19, 1993; presented as Paper 93-1399 at the AIAA/ASME/ASCE/AHS/ASC 34th Structures, Structural Dynamics, and Materials Conference, La Jolla, CA, April 19-21, 1993; accepted for publication April 27, 1993.

*Assistant Professor, Department of Mechanical, Aerospace, and Manufacturing Engineering. Member AIAA.

†Research Assistant, Department of Mechanical, Aerospace, and Manufacturing Engineering.

where α, ξ, ζ, η, W, and λ are constants, and κ_x, κ_y, and κ_{xy} are the laminate curvatures ($= -\partial^2 w/\partial x^2, -\partial^2 w/\partial y^2, -2\partial^2 w/\partial x \partial y$) that appear in the laminated plate equations[11]

$$\begin{Bmatrix} N_x \\ N_y \\ N_{xy} \\ M_x \\ M_y \\ M_{xy} \end{Bmatrix} = \begin{bmatrix} A_{11} & A_{12} & A_{16} & B_{11} & B_{12} & B_{16} \\ A_{12} & A_{22} & A_{26} & B_{12} & B_{22} & B_{26} \\ A_{16} & A_{26} & A_{66} & B_{16} & B_{26} & B_{66} \\ B_{11} & B_{12} & B_{16} & D_{11} & D_{12} & D_{16} \\ B_{12} & B_{22} & B_{26} & D_{12} & D_{22} & D_{26} \\ B_{16} & B_{26} & B_{66} & D_{16} & D_{26} & D_{66} \end{bmatrix} \begin{Bmatrix} \epsilon_x^0 \\ \epsilon_y^0 \\ \gamma_{xy}^0 \\ \kappa_x \\ \kappa_y \\ \kappa_{xy} \end{Bmatrix} \tag{3}$$

Employing the compatibility equations, the large-deformation plate equilibrium equations, and the kinematical constraint that the total shortening of the delaminated region—due to midplane straining and geometrical effects—equals the shortening of the base region due only to midplane straining, the following values are obtained[3]

$$W = \frac{4}{\lambda}(\epsilon_0 - \epsilon_{cr})^{1/2} \tag{4}$$

$$\alpha = -\epsilon_{cr} = -(\lambda^2 D^* + A_{12}\beta + A_{16}\gamma)/A_{11} \tag{5}$$

$$\xi = -(A_{16}\eta - B_{11}W\lambda^2/2)/A_{11} \tag{6}$$

$$\eta = \frac{W\lambda^2}{2}\begin{vmatrix} A_{11} & B_{11} \\ A_{16} & B_{16} \end{vmatrix}\left(\begin{vmatrix} A_{11} & A_{16} \\ A_{16} & A_{66} \end{vmatrix}\right)^{-1} \tag{7}$$

$$\zeta = 0 \tag{8}$$

where

$$D^* \equiv \begin{vmatrix} A_{11} & A_{16} & B_{11} \\ A_{16} & A_{66} & B_{16} \\ B_{11} & B_{16} & D_{11} \end{vmatrix}\left(\begin{vmatrix} A_{11} & A_{16} \\ A_{16} & A_{66} \end{vmatrix}\right)^{-1} \tag{9}$$

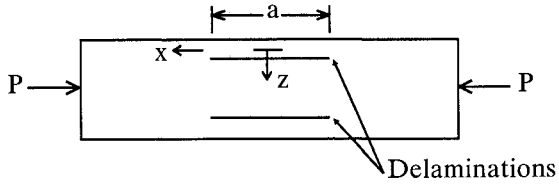

Fig. 1 Laminate with two symmetrically located delaminations.

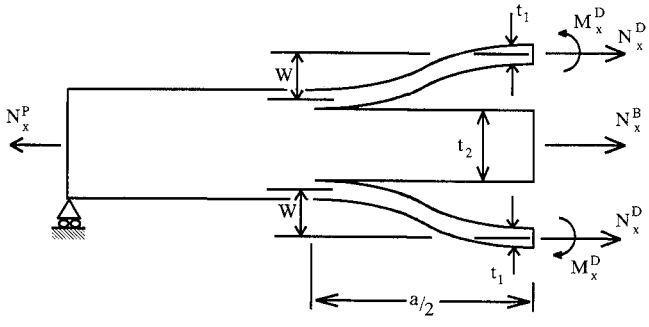

Fig. 2a Post-buckled shape, showing internal load and moment resultants.

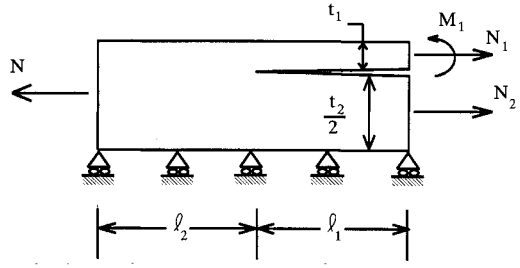

Fig. 2b Crack tip element and local loading.

The critical strain is ϵ_{cr}, i.e., it is the magnitude of the strain in the x direction, in the base region, when the delaminated region buckles. All A_{ij}, B_{ij}, and D_{ij} in the preceding equations are for the delaminated region.

Finally, to satisfy the zero-slope boundary conditions at the delamination tips $x = \pm a/2$

$$\lambda = 2\pi/a \tag{10}$$

Crack Tip Element Analysis

Figure 2a shows one-half of the laminate in its postbuckled state. In the figure and text that follow, the superscript D is used to denote quantities for the delaminated region, B is used for the base region, and P is used for the parent laminate. The forces and moments depicted in the figure are internal force and moment resultants for the delaminated and base regions at $x = 0$ and for the parent laminate in the "far-field."

By symmetry, the loads in each of the delaminated regions N_x^D are equal, the moments M_x^D are equal and opposite (as shown), and the moments in the base region and parent laminate are zero. Substituting Eq. (2) into the expression for N_x^D given by Eq. (3), using Eqs. (5) and (6) and evaluating the result at $x = 0$ gives

$$N_x^D = -\lambda^2 D^* \tag{11}$$

where D^* is given by Eq. (9) and is evaluated using the properties of the delaminated region. Equation (11) indicates that, regardless of the far-field load, the buckled, delaminated region carries only its local buckling load. In a similar manner, the in-plane load acting on the base region at $x = 0$ is found to be

$$N_x^B = -A_{11}^B\epsilon_0 + A_{12}^B\beta + A_{16}^B\gamma \tag{12}$$

and, by equilibrium considerations

$$N_x^P = 2N_x^D + N_x^B \tag{13}$$

The moments acting on the delaminated regions at $x = 0$ are found by substituting Eq. (2) into Eq. (3) to obtain

$$M_x^D = B_{11}^D(\alpha + \xi) + B_{12}^D\beta + B_{16}^D(\gamma + \eta) - D_{11}^D W\lambda^2/2 \tag{14}$$

Figure 2b shows the crack tip element and local loading. The crack tip element approach to predicting mixed-mode energy release rates was first introduced in Ref. 9. The element is assumed to be "cut" from the laminate very near the crack tip. It is assumed that the length of the cracked and uncracked sections of the element, ℓ_1 and ℓ_2, respectively, are large with respect to the element thickness, but are sufficiently small that geometric nonlinearities are negligible. Thus, classical laminated plate theory may be used to predict the deformation, strain energy, and energy release rate of the crack tip element. The effect of the geometric nonlinearities is wholly accounted for through the loading on the element. Note that global midplane symmetry is exploited in the element formulation.

By comparison with Fig. 2a, the loads acting on the crack tip element are given by

$$\begin{aligned} N_1 &= N_x^D & N_2 &= N_x^B/2 \\ N &= N_1 + N_2 & M_1 &= M_x^D - N_x^D W \end{aligned} \tag{15}$$

The energy release rate of the crack tip element is obtained through a modified virtual crack closure method and is expressed in terms of a concentrated crack tip shear force N_c and moment M_c. The concentrated crack tip force and moment are obtained through classical plate theory and fully characterize that portion of the loading on the crack tip element that produces the stress intensity factor.[9,10] Thus, the energy release rate of the element may be expressed in terms of only two

parameters, namely N_c and M_c, rather than the three quantities N_1, N_2, and M_1.

By linearity, the complex stress intensity factor may be expressed as a linear combination of N_c and M_c. This operation introduces two unknown constants. These constants are obtained by comparing the expression for the total energy release rate, as derived from the stress intensity factor, to that obtained through virtual crack closure. For fracture problems in which crack growth is between orthotropic layers and the crack tip stress field exhibits an inverse square root singularity, the following equations are obtained[9,10]:

$$g_1 = \sqrt{2G_1} = -N_c\sqrt{c_1}\sin\Omega + M_c\sqrt{c_2}\cos(\Omega+\Gamma) \tag{16}$$

$$g_2 = \sqrt{2G_{II}} = N_c\sqrt{c_1}\cos\Omega + M_c\sqrt{c_2}\sin(\Omega+\Gamma) \tag{17}$$

where g_1 and g_2 are proportional to the mode I and mode II stress intensity factors, respectively. From Eqs. (16) and (17), the total energy release rate G is given by

$$G = G_I + G_{II} \tag{18}$$

where

$$G_I = \tfrac{1}{2}g_1^2 \qquad G_{II} = \tfrac{1}{2}g_2^2 \tag{19}$$

The expressions for the concentrated crack tip force N_c and moment M_c for the case where there is no moment in the parent laminate and the parent laminate possesses midplane symmetry is given by[9,10]

$$N_c = -N_1 + A_1A'N \tag{20}$$

$$M_c = M_1 - N_1t_1/2 + (A_1t_1/2 - B_1)A'N \tag{21}$$

The values of A, B, D, A', B', and D' used earlier, without subscripts, refer to the parent laminate; when the subscript "1" is used, they refer to the delaminated region; and when the subscript "2" is used, they refer to the base region. For any of these regions, it is assumed that the laminated plate equations [see Eq. (3)] may be written as

$$\begin{aligned} N &= A\epsilon_x^0 + B\kappa_x \\ M &= B\epsilon_x^0 + D\kappa_x \end{aligned} \tag{22}$$

Or, in their inverted form

$$\begin{aligned} \epsilon_x^0 &= A'N + B'M \\ \kappa_x &= B'N + D'M \end{aligned} \tag{23}$$

If A, B, D, A', B', and D' are unsubscripted, then ϵ_x^0, κ_x, N, and M are for the parent laminate. For the delaminated region, A, B, D, A', B', D', N, and M in Eqs. (22) and (23) are all given the subscript "1." For the base region, A, B, D, A', B', D', N, and M in Eqs. (22) and (23) are all given the subscript "2." Thus, if the laminate is in a state of plane strain ($\beta = \gamma = 0$)

$$\begin{aligned} A &= A_{11}^P & A_1 &= A_{11}^D & A_2 &= A_{11}^B \\ B &= B_{11}^P & B_1 &= B_{11}^D & B_2 &= B_{11}^B \\ D &= D_{11}^P & D_1 &= D_{11}^D & D_2 &= D_{11}^B \end{aligned} \tag{24}$$

and A', B', and D' for the different regions are found by inverting Eq. (22). If the laminate is in a state of plane stress ($\beta = \nu_{xy}^P\epsilon_0$, $\gamma = \nu_{xs}^P\epsilon_0$)

$$A' = \alpha_{11}^P \qquad B' = \beta_{11}^P \qquad D' = \delta_{11}^P \tag{25}$$

where α_{11} is the element in the first row, first column, β_{11} is the element in the first row, fourth column, and δ_{11} is the element in the fourth row, fourth column of the inverse of the coefficient matrix (for the parent laminate) of Eq. (3). A_1', A_2', B_1', B_2', D_1', and D_2' are defined in an analogous manner for the delaminated and base regions. For plane stress, A, B, and D for each of the regions are found by inverting Eq. (23); ν_{xy}^P and ν_{xs}^P are the major Poisson's ratio and in-plane shear Poisson's ratio of the parent laminate, defined by

$$\nu_{xy}^P = \begin{vmatrix} A_{12}^P & A_{26}^P \\ A_{16}^P & A_{66}^P \end{vmatrix} \left(\begin{vmatrix} A_{22}^P & A_{26}^P \\ A_{26}^P & A_{66}^P \end{vmatrix} \right)^{-1} \tag{26}$$

$$\nu_{xs}^P = \begin{vmatrix} A_{22}^P & A_{12}^P \\ A_{26}^P & A_{16}^P \end{vmatrix} \left(\begin{vmatrix} A_{22}^P & A_{26}^P \\ A_{26}^P & A_{66}^P \end{vmatrix} \right)^{-1} \tag{27}$$

The values of Γ, c_1, and c_2 used in Eqs. (16) and (17) are given by[9,10]

$$\sin\Gamma = \frac{c_{12}}{\sqrt{c_1c_2}} \tag{28}$$

where

$$\begin{aligned} c_1 &= A_1' + A_2' + B_1't_1 - B_2't_2 + D_1't_1^2/4 + D_2't_2^2/4 \\ c_2 &= D_1' + D_2' \\ c_{12} &= D_2't_2/2 - D_1't_1/2 - B_1' - B_2' \end{aligned} \tag{29}$$

and t_1 and t_2 are the thicknesses of the delaminated and base regions, respectively, as shown in Fig. 2.

The value of Ω is independent of the loading and must be taken from a continuum analysis or other results from one special loading case.[9,10] For many cases, Ω may be taken directly from Ref. 10, which gives this parameter as a function of material property and thickness ratios of the cracked regions. Also, the total energy release rate, as given by Eq. (18), is independent of the value of Ω. Thus, setting $\Omega = 0$ is a simple means of determining the total energy release rate and of identifying trends in the mode ratio.[12]

The previous results are for a general crack tip element.[9,10] To enforce the symmetry condition of Fig. 2b, namely that the base region does not bend, take $D_2' = 0$. Further, since only one-half of the parent laminate and of the base region are considered in the crack tip element shown in Fig. 2b, take $A' = 2A'$ of the full, symmetric parent laminate, and take $A_2' = 2A_2'$ of the full, symmetric base region. Note that as a result of global symmetry, $B_2' = 0$.

Finally, note that when the effective stiffness of the base region becomes very large as compared with that of the delaminated region, the crack tip element analysis gives results for the "thin film" case.[1-3]

Finite Element Verification

Homogeneous Orthotropic Material

The first case considered is that of a homogeneous orthotropic material. The material properties of the base and delaminated regions are equivalent and are given in Table 1. The delaminated regions are each 0.4 mm thick, and the base region is 8.0 mm thick. The delamination length a (see Fig. 1) is 30 mm. The laminate is assumed to be in a state of plane strain (i.e., $\beta = \gamma = 0$). Energy release rates and fracture mode ratios for this particular laminate have previously been evaluated using a nonlinear finite element analysis.[13]

Equation (5) may be used to evaluate the delamination buckling strain; for the material properties given in Table 1 and the previously specified thicknesses and delamination length, this gives

$$\epsilon_{cr} = \lambda^2\frac{D_{11}^D}{A_{11}^D} = \frac{\pi^2t_1^2}{3a^2} = 585\ \mu\text{m/m} \tag{30}$$

The loading on the crack tip element is given by Eqs. (11-15). Equations (4-10) allow this loading to be expressed solely in terms of the base region strain ϵ_0. Thus, using these expres-

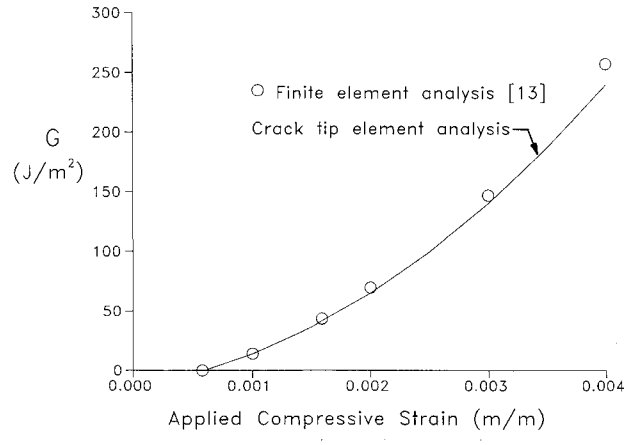

Fig. 3a Total energy release rate as predicted by nonlinear finite element and crack tip element analyses—homogeneous orthotropic material.

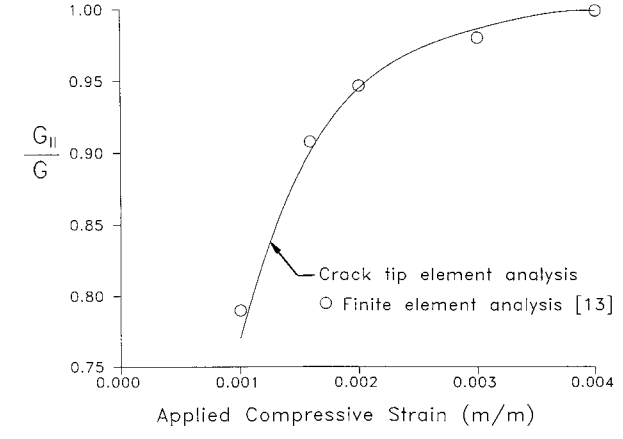

Fig. 3b Fracture mode ratio as predicted by nonlinear finite element and crack tip element analyses—homogeneous orthotropic material.

sions along with Eqs. (16–21) allows the energy release rate and individual mode I and mode II components to be expressed as a function of the base region strain. However, the results for G, G_I, and G_{II} reported in Ref. 13 are in terms of the "applied compressive strain" ϵ_a. This value is defined such that the applied displacement at the uncracked end of the finite element model u_a is given by

$$u_a = \epsilon_a L \tag{31}$$

where L is the total length of the model. That is, in this reference, the finite element model was essentially a discretization of Fig. 2b. The model was fixed, with respect to in-plane displacements, at the cracked end (the right end in Fig. 2b) and the uncracked end was subjected to incrementally increasing in-plane compressive displacements u_a. The total model length L ($\ell_1 + \ell_2$ in Fig. 2b) was 50 mm.[14] The half-crack length ℓ_1 was 15 mm. To relate the applied compressive strain ϵ_a to the base region strain ϵ_0, break the total displacement up into the sum of the displacement in the parent laminate plus that in the region containing the delamination, i.e.,

$$\epsilon_a L = \epsilon_a(\ell_1 + \ell_2) = \epsilon_0 \ell_1 + \epsilon_P \ell_2 \tag{32}$$

where ϵ_P is the magnitude of the strain in the parent laminate. Now use Eqs. (23) to express ϵ_P in terms of the load in the parent laminate N_x^P and use Eq. (13), $N_x^P = 2N_x^D + N_x^B$, where N_x^D is given by Eq. (11) and N_x^B is given by Eq. (12). Also, use the fact that the delaminated region, base region, and parent laminate are all symmetric about their own midplane and are in a state of plane strain, to obtain

$$\epsilon_P = (2\lambda^2 D_{11}^D + A_{11}^B \epsilon_0)/A_{11}^P \tag{33}$$

Substituting Eq. (33) into Eq. (32) gives the base region strain in terms of the applied compressive strain as

$$\epsilon_0 = \frac{\epsilon_a(\ell_1 + \ell_2) - 2\lambda^2 \ell_2 D_{11}^D / A_{11}^P}{\ell_1 + \ell_2 A_{11}^B / A_{11}^P} \tag{34}$$

Using Eq. (34) and the preceding results, the energy release rate, as predicted by the crack tip element approach, may now be expressed in terms of the applied strain for direct comparison to the nonlinear finite element results. This comparison is presented in Figs. 3a and 3b. Note from these figures that essentially the same results are predicted for the total energy release rate and fracture mode ratio by the two methods. The value of Ω used for the crack tip element predictions in the figures was taken from Ref. 10; for the material properties given in Table 1, this reference gives $\Omega = 20$ deg.

Note from Fig. 3b that the energy release rate becomes pure mode II at an applied strain of approximately 0.004. For strains larger than this value, the mode I stress intensity factor becomes negative, and the mode I energy release rate is actually a closing mode. That is, for $\epsilon_a > 0.0043$ m/m, the crack tip element analysis predicts $g_I < 0$ [see Eq. (16)]. For the finite element analysis, crack face interpenetration is predicted for applied strains greater than this value. To obtain accurate energy release rates beyond this point, crack face contact restraints are required within the nonlinear finite element analysis.

It should also be pointed out that, in the approximate superposition analysis,[6] it is assumed that the strains in the parent laminate and base region are equal. If the correspondence between these values as given by Eqs. (31–34) is used, the approximate superposition analysis gives the same results as the crack tip element approach. The approximate superposition analysis does not, however, account for the possibility of various coupling behaviors (i.e., bending-stretching, stretching-shearing, or bending-shearing) in the delaminated or base regions. It is therefore only applicable, with the previous modification, to the case in which A_{16}, B_{11}, and B_{16} of the delaminated and base regions are zero. Conversely, the crack tip element approach may be thought of as the generalization of this earlier analysis.

Graphite/Epoxy Laminate

The second case considered is that of a $[0_2/90/0_2]_{3s}$ graphite/epoxy laminate with delaminations at the interfaces of the fifth and sixth and the 25th and 26th plies. The delamination length a was taken equal to 50.8 mm. The laminate is assumed to be in a state of plane strain. Unidirectional material properties for the graphite/epoxy are given in Table 2. Energy release rates and fracture mode ratios for this laminate were obtained by nonlinear finite element analysis using ABAQUS 4-9-1, licensed from Hibbitt, Karlsson, and Sorensen, Inc.

Table 1 Material properties for homogeneous, orthotropic material

$E_{11} = 52.58$ GPa	$\nu_{12} = 0.305$	$G_{12} = 20.14$ GPa
$E_{22} = 52.58$ GPa	$\nu_{13} = 0.330$	$G_{13} = 4.48$ GPa
$E_{33} = 12.66$ GPa	$\nu_{23} = 0.330$	$G_{23} = 4.48$ GPa

Table 2 Unidirectional material properties for graphite/epoxy[a]

$E_{xx} = 124.11$ GPa	$\nu_{xy} = 0.37$	$G_{xy} = 5.45$ GPa
$E_{yy} = 10.34$ GPa	$\nu_{xz} = 0.37$	$G_{xz} = 5.45$ GPa
$E_{zz} = 10.34$ GPa	$\nu_{yz} = 0.35$	$G_{yz} = 3.86$ GPa

[a]Single ply thickness: 1.27×10^{-4} m.

Model Description

Similar to that described earlier, the finite element model that we developed was essentially a discretization of Fig. 2b. That is, symmetry with respect to the x and z axes was exploited, allowing only one-quarter of the full geometry of Fig. 1 to be modeled. The half-crack length ℓ_1 was 25.4 mm, and the overall model length $\ell_1 + \ell_2$ was 73.0 mm. The model is shown in Fig. 4. Except for the more refined region in the crack tip neighborhood, we used 15 elements through the thickness of the model, i.e., one element per ply. The aspect (length-to-width) ratio of all elements was kept below 6.25. The model contained 2126 elements and 13,608 global degrees of freedom. Eight node, biquadratic, plane strain continuum elements were used.

Figure 5 presents a plot of the finite element mesh in the crack tip region. The elements at the crack tip are square, and the element size Δ/h is equal to 0.25, where Δ is the length of the element and h is the single ply thickness. This accuracy of this near tip meshing method is demonstrated in Ref. 10. This reference presents convergence studies and comparisons of energy release rates and mode ratios as obtained by this mesh to those obtained by more conventional meshing methods.[5,6,9,13] This meshing method predicts the same results as conventional methods; however, fewer elements are required.[10] Also, it is very simple to refine this mesh locally at the crack tip. For example, in our mesh refinement studies, we considered element sizes at the crack tip as small as Δ/h equal to 0.125; this more refined mesh gave energy release rates and fracture mode ratios within 0.4 percent of those obtained from the mesh pictured.

Referring to Fig. 2b, symmetry boundary conditions were prescribed by constraining displacements with respect to x along the right edge (i.e., the edge containing the crack) of the model and by constraining displacements with respect to z along the lower surface. Displacements were applied in the x direction along the left (uncracked) edge of the model; all nodes along this edge were constrained to displace by the same amount. Initially, a linear buckling analysis was performed. The deflected shape, as predicted by the buckling analysis, was reduced by 99.9 percent and used as an initial imperfection in a second run to obtain postbuckling response. Displacements, along the left edge, were applied incrementally, and the equilibrium equations, with respect to the deformed geometry, were solved at each increment. Energy release rate components were obtained by the virtual crack closure technique.[15]

Fig. 4 Finite element model.

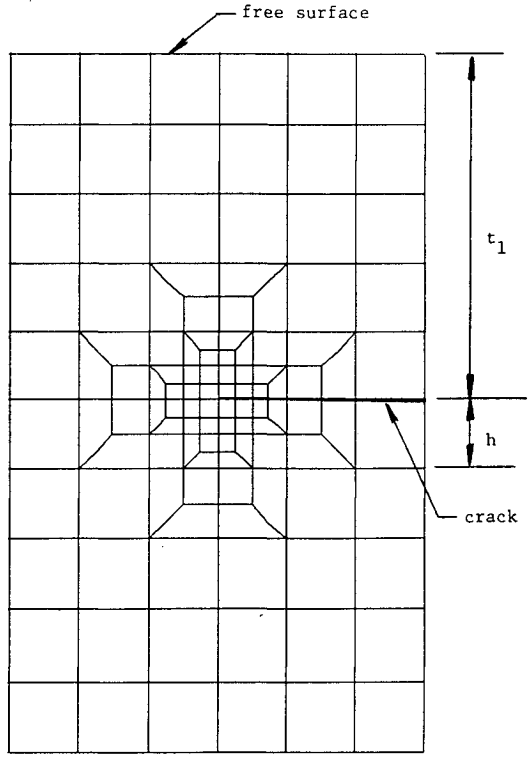

Fig. 5 Near tip region of finite element model.

Determination of Ω

For this particular geometry, we determined Ω by a single *linear* finite element analysis of the crack tip element geometry. As described in previous works,[9,10] a loading was chosen that 1) created no forces and moments in the parent laminate and 2) caused $M_c = 0$. The loading we chose was $N_1 = 17{,}513$ N/m, $N_2 = -17{,}513$ N/m and $M_1 = 5.56$ Nm/m; using the virtual crack closure technique,[15] we obtained $G_I = 0.59$ J/m^2 and $G_{II} = 8.81$ J/m^2. By Eq. (16), for this particular loading

$$\sin\Omega = -\sqrt{2G_I}/N_c\sqrt{c_1} \tag{35}$$

which gives $\Omega = 14.6$ deg.

Results

Similar to that done for the previous case, Eqs. (31-34) were used to compare the energy release rate and mode ratio as predicted by the nonlinear finite element and crack tip element analyses as a function of the applied compressive strain. These comparisons are presented in Figs. 6a and 6b. As for the

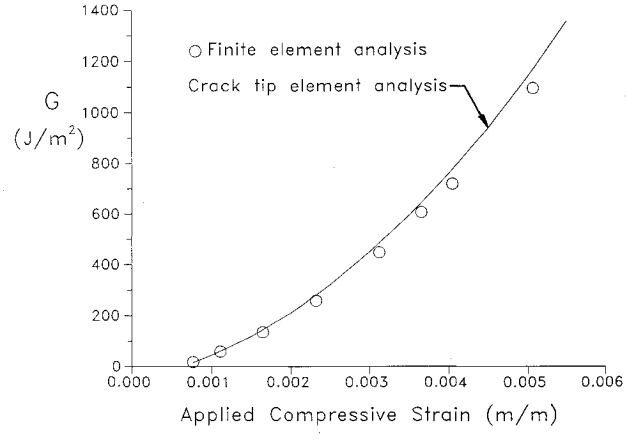

Fig. 6a Total energy release rate as predicted by nonlinear finite element and crack tip element analyses—$[0_2/90/0_2]_{3s}$ laminate.

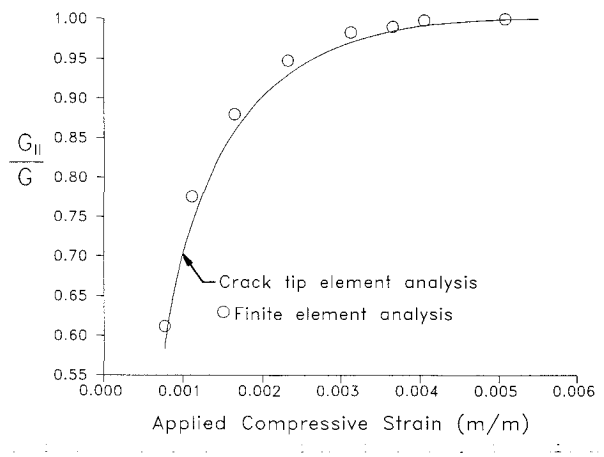

Fig. 6b Fracture mode ratio as predicted by nonlinear finite element and crack tip element analyses—$[0_2/90/0_2]_{3s}$ laminate.

Fig. 7a Deformed mesh plot at an applied strain of 0.00111 m/m.

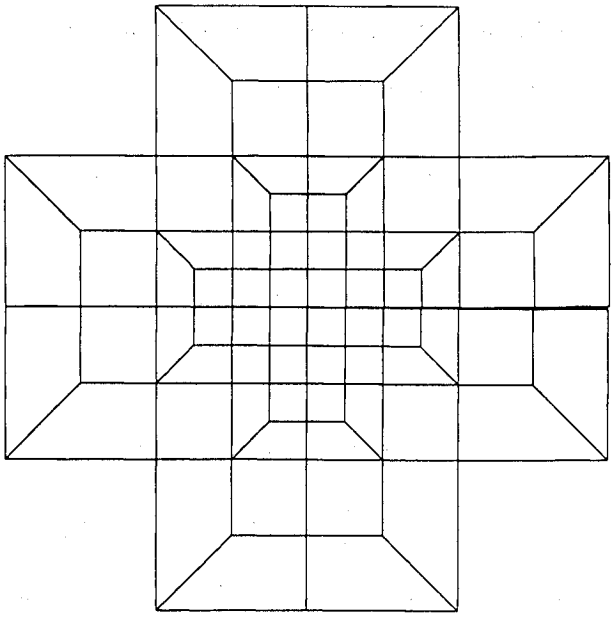

Fig. 7b Deformation of crack tip region at an applied strain of 0.00111 m/m.

Fig. 7c Deformed mesh plot at an applied strain of 0.00405 m/m.

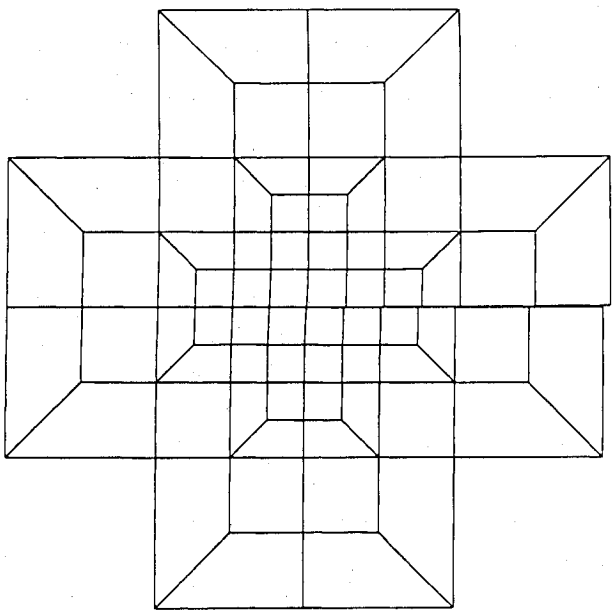

Fig. 7d Deformation of crack tip region at an applied strain of 0.00405 m/m.

previous case, essentially the same results are obtained by the two methods. Also as in the previous case, the energy release rate is seen to be predominantly mode II, with the ratio G_{II}/G increasing with increasing applied compressive strain. This is further illustrated in Fig. 7. Figure 7a presents a deformed mesh plot, and Fig. 7b shows a plot of the crack tip region at an applied strain of 0.00111 m/m. Note From Fig. 7b that both opening and shearing mode deformations are evident. The mode ratio G_{II}/G at this strain level was 0.77. Figures 7c and 7d show plots of the full deformed mesh and of the crack tip region at an applied strain of 0.00405 m/m. This corresponded to a mode ratio of 0.99. As would be expected, a comparison of Figs. 7a and 7c indicates that the global separation of the crack faces increases with increasing applied strain. A comparison of Figs. 7b and 7d indicates that, as the applied strain increases, the local deformation transitions to a predominantly shearing mode. This transition occurs because the difference in midplane strain between the delaminated and base regions becomes more pronounced. That is, the delaminated and base regions must shorten by the same amount. As the applied strain increases, all shortening of the base region occurs as a result of midplane straining. However, in its postbuckled state, the load in the delaminated region does not increase [see Eq. (11)] and all shortening occurs due to the geometrical effect associated with the out-of-plane deformation.

As the applied strain continues to increase, $G_{II}/G \rightarrow 1$, the crack faces continue to close and crack face contact, followed by interpenetration, is observed. The crack tip element analysis predicts crack face contact will occur at an applied strain of 0.0056 m/m. Because we did not obtain finite element output at each increment of applied strain (this would have made our output files unmanageably large), we could not verify this prediction exactly. However, from the output we did obtain, crack face contact was predicted to occur between an applied strain of 0.0051 and 0.0061 m/m. Considering the excellent correlation between crack tip element and finite element results evidenced in Figs. 6a and 6b, it is likely that predictions of crack face contact by the two methods were consistent.

Conclusions

A new approach has been presented to predict mixed-mode energy release rates in the one-dimensional delamination buckling problem. This approach uses a closed form, nonlinear cylindrical buckling analysis to obtain the force and moment resultants in the base laminate, parent laminate, and postbuckled delaminated region, and a closed form, crack tip element analysis to determine energy release rate and fracture mode ratio. It has been shown that this new approach gives the same results as geometrically nonlinear finite element analyses.

The crack tip element approach does not completely eliminate the need for finite element analyses; rather, one finite element analysis must still be performed to get the unknown coefficient Ω. It has been shown in previous works[9,10] that it is simplest and most accurate to obtain this coefficient by performing a finite element analysis of the crack tip element under one special loading case chosen such that $M_c = 0$. However, only a single *linear* run need be performed; this new approach obviates the need for nonlinear analyses. Further, this linear analysis need only be of the crack tip region; the full, cracked geometry need not be modeled.[10] Also, for many practical geometries, the value of Ω may be found in a recently published work.[10] If one does not wish to perform any finite element work, and the value of Ω cannot be taken directly from Ref. 10, setting $\Omega = 0$ is a useful means of identifying general trends in mode ratio; this approach will also give correct results for total energy release rate. In fact, this approach is wholly sufficient for those material systems where the fracture toughness does not exhibit fracture mode ratio dependence.

For many practical problems involving instability-related delamination growth, delamination growth occurs between plies with dissimilar orientations. For this case, with linear elastic material properties, a crack tip oscillating singularity is predicted to exist, and a fracture mode ratio cannot be uniquely defined.[12] The effect on the crack tip element analysis is that a unique value of Ω cannot be obtained. That is, the value of Ω, as obtained from a linear finite element analysis, will not converge with increasing amounts of mesh refinement. It was proposed in a previous work[12] that, for these

cases, one of Dundurs' generalized parameters for the specific interfacial region containing the crack be taken equal to zero in the numerical model. This method provides a relatively simple means of eliminating the problems associated with the oscillating singularity while still obtaining physically meaningful results.

Finally, the crack tip element approach to obtain energy release rate and mode ratio has been applied herein to the problem of delamination buckling. However, the general formulation developed in Refs. 9 and 10 allows this approach to be applied to virtually any delamination problem of practical interest. Along with the proposed method of eliminating the difficulties associated with the oscillating stress singularity,[12] this approach offers a powerful means of solving a wide variety of delamination growth problems. For example, it has recently been shown that this approach may be used to predict mixed-mode energy release rates in the free edge delamination problem for mechanical, hygrothermal, or combined loadings.[12]

References

[1]Chai, H., Babcock, C. D., and Knauss, W. G., "One Dimensional Modeling of Failure in Laminated Plates by Delamination Buckling," *International Journal of Solids and Structures,* Vol. 17, No. 11, 1981, pp. 1069–1083.

[2]Yin, W. L., "Cylindrical Buckling of Laminated and Delaminated Plates," *Proceedings of the AIAA/ASME/ASCE/AHS 27th Structures, Structural Dynamics, and Materials Conference* (San Antonio, TX), AIAA, New York, 1986, pp. 165–179.

[3]Yin, W. L., "The Effects of Laminated Structure on Delamination Buckling and Growth," *Journal of Composite Materials,* Vol. 22, June 1988, pp. 502–517.

[4]Rothschilds, R. J., Gillespie, J. W., Jr., and Carlson, L. A., "Instability-Related Delamination Growth in Thermoset and Thermoplastic Composites," *Composite Materials: Testing and Design (Eighth Conference),* ASTM STP 972, edited by J. D. Whitcomb, American Society for Testing and Materials, Philadelphia, PA, 1988, pp. 161–179.

[5]Whitcomb, J. D., "Analysis of Instability-Related Delamination Growth of a Through-Width Delamination," NASA-TM-86301, Sept. 1984.

[6]Whitcomb, J. D., "Strain Energy Release Rate Analysis of Cyclic Delamination Growth in Compressively Loaded Laminates," NASA-TM-84598, Jan. 1983.

[7]Donaldson, S. L., "The Effect of Interlaminar Fracture Properties on the Delamination Buckling of Composite Laminates," *Composites Science and Technology,* Vol. 28, No. 1, 1987, pp. 33–44.

[8]Johnson, W. S., and Mangalgiri, P. D., "Influence of the Resin on Interlaminar Mixed-Mode Fracture," *Toughened Composites,* ASTM STP 937, edited by N. J. Johnston, American Society for Testing and Materials, Philadelphia, PA, 1987, pp. 295–315.

[9]Schapery, R. A., and Davidson, B. D., "Prediction of Energy Release Rate for Mixed-Mode Delamination using Classical Plate Theory," *Applied Mechanics Reviews,* Vol. 43, No. 5, Pt. 2, 1990, pp. S281–S287.

[10]Davidson, B. D., Hu, H., and Schapery, R. A., "A Crack Tip Element for Layered Elastic Plater," *Journal of Applied Mechanics* (to be published).

[11]Whitney, J. M., *Structural Analysis of Laminated Anisotropic Plates,* Technomic Publishing, Westport, CT, 1987, Chap. 2.

[12]Davidson, B. D., "Prediction of Energy Release Rate for Edge Delamination Using a Crack Tip Element," *Fifth American Society for Testing and Materials Symposium on Composite Materials: Fatigue and Fracture* (Atlanta, GA), American Society for Testing and Materials, Philadelphia, PA, May, 1993.

[13]Whitcomb, J. D., "Mechanics of Instability-Related Delamination Growth," *Composite Materials: Testing and Design (Ninth Volume),* ASTM STP 1059, edited by S. P. Garbo, American Society for Testing and Materials, Philadelphia, PA, 1990, pp. 215–230.

[14]Whitcomb, J. D., private communication, Texas A&M University, 1992.

[15]Rybicki, E. F., and Kanninen, M. F., "A Finite Element Calculation of Stress Intensity Factors by a Modified Crack Closure Integral," *Engineering Fracture Mechanics,* Vol. 9, 1977, pp. 931–938.